Impact of Multiple Phase Transitions in Dense QCD on Compact Stars

Armen Sedrakian
Institute for Theoretical Physics, Wrocław University
Frankfurt Institute for Advanced Studies

Many-Particle Systems under Extreme Conditions
Polish-German WE-Heraeus-Seminar

5 December 2023

Uniwersytet Wrocławski

Towards the phase diagram of low-temperature QCD

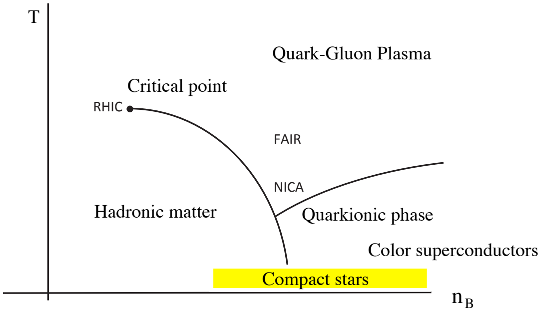

Scketch of the phase diagram of strongly interacting matter in the temperature and baryonic density plain. Compact stars cover the low-temperature and high-density regime of this phase diagram. The parameter ranges covered by the FAIR, NICA, and RHIC facilities are also indicated.

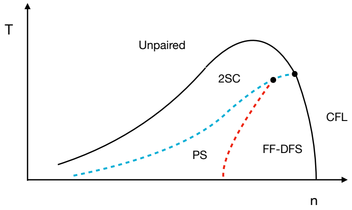

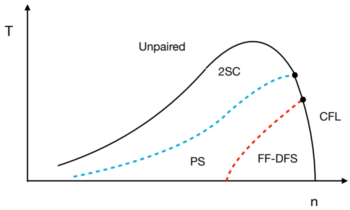

Sketch of the phase diagram of strongly interacting matter in the temperature and baryonic density

- (a) The "2SC" phase (the abbrivation refereing to two-superconducting-colors)

$$\Delta_{2SC} \propto \langle \psi^T(x) C\gamma_5 \tau_2 \lambda_2 \psi(x) \rangle \neq 0, \quad 0 \leq \delta\mu < \Delta/\sqrt{2},$$

- (b) Phases with broken space symmetries

$$\Delta_{2SC} \neq 0, \quad \delta\mu > \Delta/\sqrt{2}, \quad \vec{P} \neq 0 \quad \text{(FF)} \qquad \delta\epsilon \neq 0 \quad \text{(DFS)}$$

- (c) Mixed phase(s)

$$\Delta_{2SC} \propto \langle \psi^T(x) C\gamma_5 \tau_2 \lambda_2 \psi(x) \rangle \neq 0, \quad \delta\mu = 0, \quad 0 \leq x_s \leq 1,$$

- (d) Color-flavor-locked phase

$$\Delta_{ud} \neq 0, \quad \Delta_{sd} \neq 0, \quad \Delta_{su} \neq 0, \quad (m_s \neq 0; \, \delta\mu \neq 0).$$

Quark-Meson-Coupling model

– Free propagators quarks and mesons

$$S^{-1}(q) = \begin{pmatrix} \not q + \mu\gamma_0 - m & \bar{\Delta} \\ \Delta & (\not q - \mu\gamma_0 + m)^T \end{pmatrix}, \quad D_{\pi/\sigma}(q) = \frac{1}{q_0^2 - \boldsymbol{q}^2 - m_{\pi/\sigma}^2},$$

– Anomalous self-energies and full propagator as a solution of Schwinger-Dyson equations

$$\Delta(k) = ig_\pi^2 \int \frac{d^4q}{(2\pi)^4} \left(-\frac{\tau^i}{2}\gamma_5\right)^T S_{21}(q)\frac{\tau^j}{2}\gamma_5\delta_{ij}D_\pi(q-k)$$
$$+ig_\sigma^2 \int \frac{d^4q}{(2\pi)^4}(-\mathbb{I})^T S_{21}(q)\mathbb{I}D_\sigma(q-k),$$
$$S_{21}(q) = -(\lambda_2\tau_2 C\gamma_5)\sum_{\pm}\left[\frac{\Delta_\pm\Lambda_\mp(q)}{q_0^2-(\epsilon_q-\mu)^2-\Delta_\pm^2}\right] = -(\lambda_2\tau_2 C\gamma_5)F_{21}(q).$$

– Quark self-energies are express through spectral functions of mesons:

$$\sum_{i=\pm}\Delta_i(k)\Lambda^i(k) = \sum_{m=\sigma\pi}\int \frac{d^4q}{(2\pi)^4}\gamma_5 F_{21}(q)\gamma_5 D_m(q-k).$$

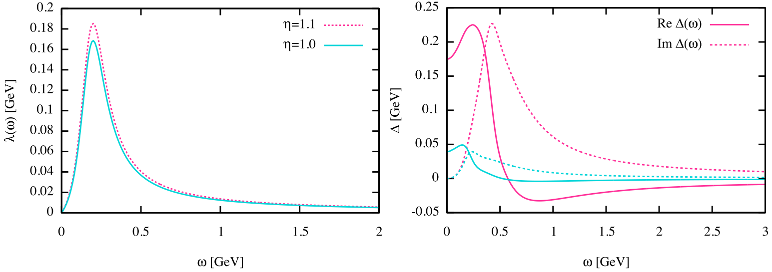

Left: The spectral function of mesons for two (dimensionless) couplings. RIght: Solutions for the real and imaginary parts of the propagators as a function of the frequency which can be then performed analytically. As a result we find

$$\Delta(k_0,k_F) = \int_0^\infty d\varepsilon\, \mathscr{F}(\varepsilon) \int_0^\infty d\omega' \lambda(\omega') \left[\frac{1}{\varepsilon + k_0 + \omega' + i\delta} + \frac{1}{\varepsilon - k_0 + \omega' - i\delta}\right],$$

$$\lambda(\omega) = \frac{g_\sigma^2 \mathscr{B}_\sigma(\omega) - 3 g_\pi^2 \mathscr{B}_\pi(\omega)}{4 v_F},$$

$$\mathscr{B}_{\pi/\sigma}(\omega) = \int_0^{2k_F} \frac{q\,dq}{(2\pi)^2} B_{\pi/\sigma}(\omega,q) K_{-+}, \quad \mathscr{F}(\varepsilon) = \mathrm{Re}\frac{\Delta(\varepsilon)\mathrm{sgn}(\varepsilon)}{[\varepsilon^2 - \Delta(\varepsilon)^2]^{1/2}}.$$

Constant Speed of Sound (CSS) approximation

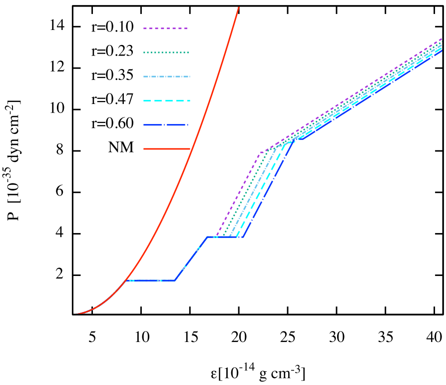

The pressure vs energy density (EoS) for nucleonic matter (solid curve) and a series of EoS which contain two sequential phase transitions via Maxwell construction manifest in the jumps of the energy density. The models differ by the magnitude of the second jump measured in terms of the ratio $r = \Delta\epsilon_2/\Delta\epsilon_1$.

Mass-Radius relation

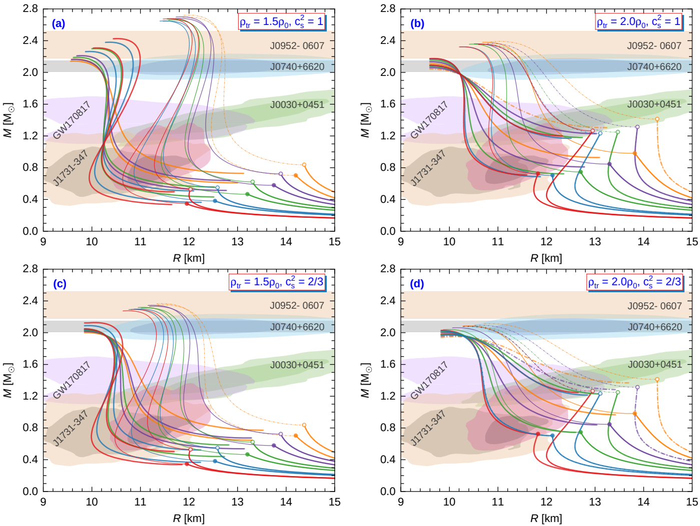

Models are built upon nucleonic models grouped by $L_{sym} = 20$, 40, 60, 80 and 100 MeV; for each, Qsat is fixed as -600 and 1000 MeV. For each nucleonic EoS, thick line denotes the hybrid model with a maximum energy jump that yields twin configurations and a branch marginally passing the mass-radius constraints for PSR J0740+6620 and J0030+0451; while thin line denotes the model with a critical value of $\Delta\epsilon$ for which a higher value leads a connected mass-radius curve.

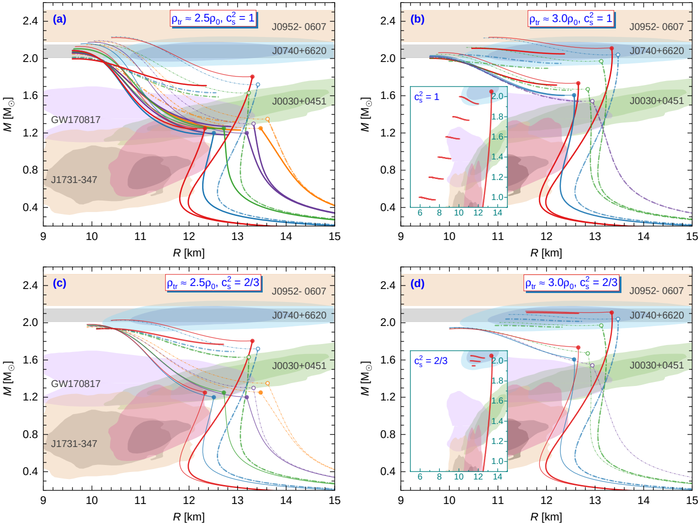

Mass-radius relations for hybrid EoS models with $\rho_{\rm tr} \simeq 2.5\rho_0$ and $3.0\ \rho_0$, for $c_s^2 = 1$ and $c_s^2 = 2/3$ for the quark phase. In each panel, the hybrid EoS models are built upon nucleonic models grouped by $L_{\rm sym} = 20$, 40, 60, 80 and 100 MeV; for each, $Q_{\rm sat}$ is chosen as an extreme value so that the resultant mass-radius curve matches marginally the inference of HESS J1731-347 (solid lines) or GW170817 (dash-dotted lines), respectively. The inset illustrates hybrid EoS models built upon an isoscalar stiff nucleonic model for case B with $c_s^2 = 1$ which could yield ultra-compact configurations.

Adding conformal fluid changes the asymptotics:

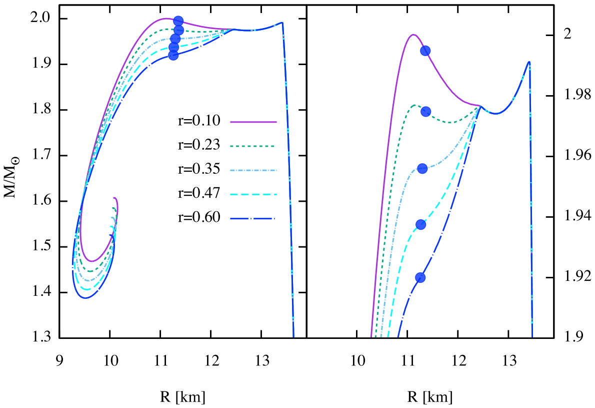

The *M*-*R* relations corresponding to the EoS with three speeds of sounds for several ratios of the second jump. The right panel enhances the high-mass range to demonstrate the emergence of the triplets and the fourth family of compact stars. Note that the different MR curves cross each other at the special point located in the low-mass and low-radius region, in analogy to the single-phase transition case. The dots indicate the density $10n_{\rm sat}$ at which the conformal fluid sets in.

150 The Equilibrium and Stability of Fluid Configurations

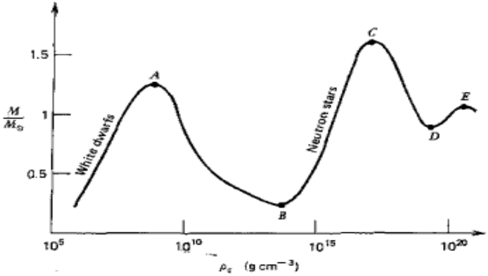

Figure 6.2 Schematic diagram showing the turning points in the mass versus central density diagram for equilibrium configurations of cold matter.

The stability is guaranteed for $dM/d\rho_c > 0$ and the star is unstable in the opposite case.

The fundamental modes of hybrid stars are obtained from the set of equations (Chandrasekhar 1964)

$$\begin{aligned} \frac{\mathrm{d}\xi}{\mathrm{d}r} &= \left(\frac{\mathrm{d}\nu}{\mathrm{d}r} - \frac{3}{r}\right)\xi - \frac{\Delta P}{r\Gamma P}, \\ \frac{\mathrm{d}\Delta P}{\mathrm{d}r} &= \left[\mathrm{e}^{2\lambda}\left(\omega^2 \mathrm{e}^{-2\nu} - 8\pi P\right) + \frac{\mathrm{d}\nu}{\mathrm{d}r}\left(\frac{4}{r} + \frac{\mathrm{d}\nu}{\mathrm{d}r}\right)\right](\rho + P)\, r\xi \\ &\quad - \left[\frac{\mathrm{d}\nu}{\mathrm{d}r} + 4\pi(\rho + P) r \mathrm{e}^{2\lambda}\right]\Delta P, \end{aligned}$$

– $\xi = \xi_{\mathrm{dim}}/r$, with ξ_{dim} Lagrangian displacement,
– ΔP the Lagrangian perturbation of pressure ,
– ρ is mass-energy density,
– ω the angular frequency, – Γ the adiabatic – Boundary conditions star center and surface:

$$\Delta P(r=0) = -3\Gamma P \xi(r=0), \qquad \Delta P(r=R) = 0.$$

– Boundary conditions at the interface:

$$[\Delta P]^{+}_{-} = 0, \qquad [\xi]^{+}_{-} = 0, \quad \text{slow conversion} \tag{1}$$

$$[\Delta P]^{+}_{-} = 0, \qquad \left[\xi - \frac{\Delta P}{r}\left(\frac{\mathrm{d}P}{\mathrm{d}r}\right)^{-1}\right]^{+}_{-} = 0. \quad \text{rapid conversion} \tag{2}$$

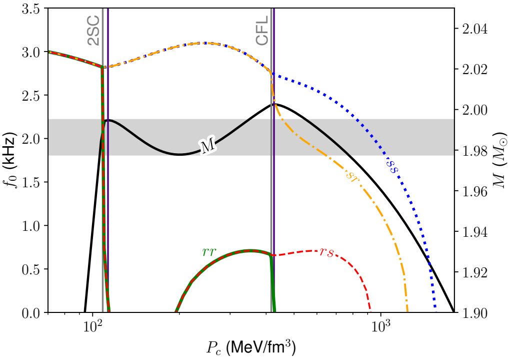

The fundamental mode of triplet stars as a function of central pressure of the configuration in the cases when both nucleonic-2SC and 2SC-CFL interfaces feature slow (solid line) or rapid conversion (dotted line). In the case of rapid conversion, the classical stability criteria apply, i.e., there are no real f_0 solutions in the region where stars are unstable. and the corresponding curves are not shown. For more details

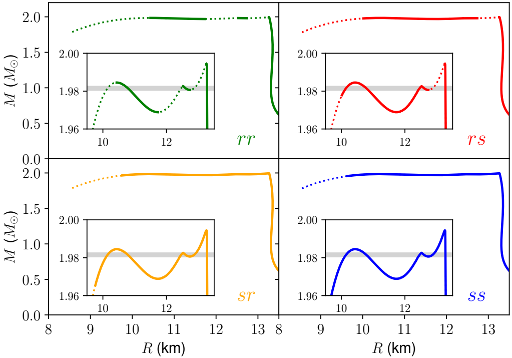

Comparison between slow and fast transitions on a sequence that features tripets in the classical case.

Gravitational Waves

TABLE I. Source properties for GW170817: we give ranges encompassing the 90% credible intervals for different assumptions of the waveform model to bound systematic uncertainty. The mass values are quoted in the frame of the source, accounting for uncertainty in the source redshift.

	Low-spin priors ($\lvert\chi\rvert \le 0.05$)	High-spin priors ($\lvert\chi\rvert \le 0.89$)
Primary mass m_1	1.36–$1.60\ M_\odot$	1.36–$2.26\ M_\odot$
Secondary mass m_2	1.17–$1.36\ M_\odot$	0.86–$1.36\ M_\odot$
Chirp mass $\mathcal{M}$	$1.188^{+0.004}_{-0.002} M_\odot$	$1.188^{+0.004}_{-0.002} M_\odot$
Mass ratio m_2/m_1	0.7–1.0	0.4–1.0
Total mass $m_{\rm tot}$	$2.74^{+0.04}_{-0.01} M_\odot$	$2.82^{+0.47}_{-0.09} M_\odot$
Radiated energy $E_{\rm rad}$	$> 0.025 M_\odot c^2$	$> 0.025 M_\odot c^2$
Luminosity distance $D_{\rm L}$	40^{+8}_{-14} Mpc	40^{+8}_{-14} Mpc
Viewing angle Θ	$\lesssim 55°$	$\lesssim 56°$
Using NGC 4993 location	$\lesssim 28°$	$\lesssim 28°$
Combined dimensionless tidal deformability $\tilde\Lambda$	≤ 800	≤ 700
Dimensionless tidal deformability $\Lambda(1.4 M_\odot)$	≤ 800	≤ 1400

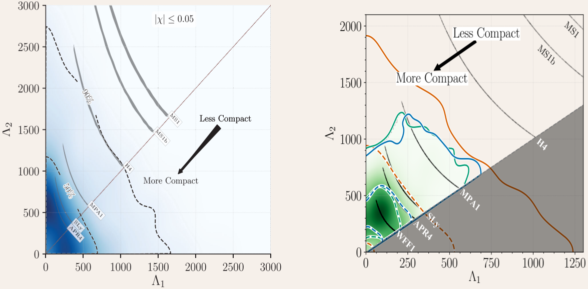

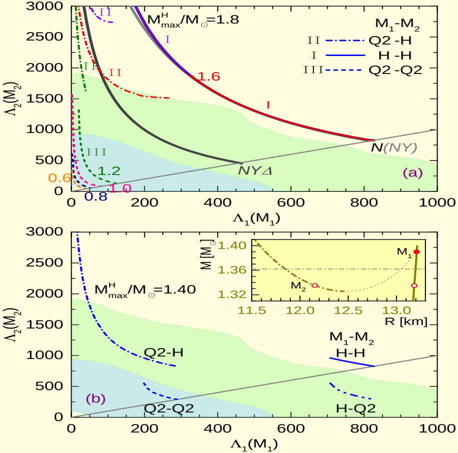

a) Tidal deformabilities of compact objects in the binary with chirp mass $\mathcal{M} = 1.186 M_\odot$ (b) Prediction by an EoS with maximal hadronic mass $M^{\rm H}_{\rm max} = 1.365 M_\odot$. The inset shows the mass-radius relation around the phase transition region. The circles M_2 are two possible companions for circle M_1, generating two points in the Λ_1-Λ_2 curves while one point is located below the diagonal line.

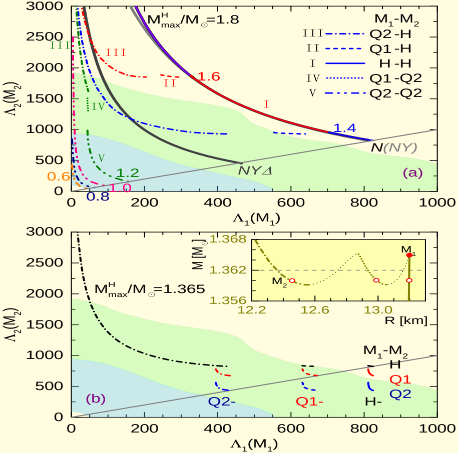

The case of double phase transition a) Tidal deformabilities of compact objects in the binary with chirp mass $\mathcal{M} = 1.186M_\odot$ (b) Prediction by an EoS with maximal hadronic mass $M^{\rm H}_{\rm max} = 1.365M_\odot$. The inset shows the mass-radius relation around the phase transition region. The circles M_2 are two possible companions for circle M_1, generating two points in the Λ_1-Λ_2 curves while one point is located below the diagonal line.

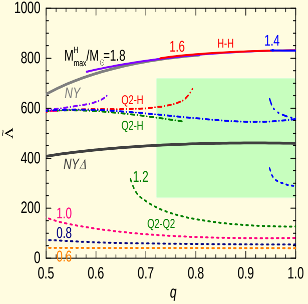

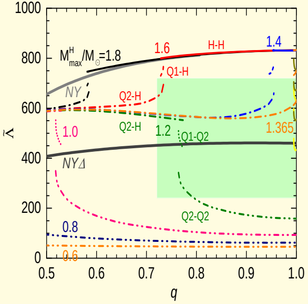

Mass weighted deformability vs. mass asymmetry for a binary system with fixed chirp mass $\mathcal{M} = 1.186 M_\odot$ predicted by a range of hybrid EoS with single phase transition and various values of $M^{\rm H}_{\rm max}$. The error shading indicates the constraints estimated from the GW170817 event and the electromagnetic transient AT2017gfo.

Conclusions

- Low-temperature QCD phase diagram is likely to have many different phases along the density / isosopin axis
- Multiple phase transition lead to multiple branches in the mass-radius diagram; asymptotics depends on how fast the conformal fluid sets in
- Gravitational wave physics will offer ways to distinguish hybrid stars via observations of tidal deformabilities